JACS
JOURNAL OF THE AMERICAN CHEMICAL SOCIETY
Article
pubs.acs.org/JACS

Macroscopic and Strong Ribbons of Functionality-Rich Metal Oxides from Highly Ordered Assembly of Unilamellar Sheets

Junyu Hou,[†] Yuanchuan Zheng,[†] Yanli Su,[†] Weikun Zhang,[‡] Tatsumasa Hoshide,[§] Feifei Xia,[#] Jiansheng Jie,[#] Qingwen Li,[‡] Zhigang Zhao,*[,‡] Renzhi Ma,[§] Takayoshi Sasaki,[§] and Fengxia Geng*[,†]

[†]College of Chemistry, Chemical Engineering and Materials Science, Soochow University, Suzhou 215123, China

[‡]Suzhou Institute of Nanotech and Nanobionics, Chinese Academy of Sciences, 398 Ruoshui Road, Suzhou Industry Park, Suzhou 215123, China

[§]International Center for Materials Nanoarchitectonics, National Institute for Materials Science, 1-1 Namiki, Tsukuba, Ibaraki 305-0044, Japan

[#]Institute of Functional Nano and Soft Materials (FUNSOM), Collaborative Innovation Center of Suzhou Nano Science and Technology, Soochow University, Suzhou 215123, China

Supporting Information

ABSTRACT: The strong interest in macroscopic graphene and/or carbon nanotube (CNT) fiber has highlighted that anisotropic nanostructured materials are ideal components for fabricating fiber assemblies. Prospectively, employing two-dimensional (2D) crystals or nanosheets of functionality-rich transition metal oxides would notably enrich the general knowledge for desirable fiber constructions and more importantly would greatly broaden the scope of functionalities. However, the fibers obtained up to now have been limited to carbon-related materials, while those made of 2D crystals of metal oxides have not been achieved, probably due to the intrinsically low mechanical stiffness of a molecular sheet of metal oxides, which is only few hundredths of that for graphene. Here, using 2D titania sheets as an illustrating example, we present the first successful fabrication of macroscopic fiber of metal oxides composed of highly aligned stacking sheets with enhanced sheet-to-sheet binding interactions. Regardless of the intrinsically weak Ti−O bond in molecular titania sheets, the optimal fiber manifested mechanical performance comparable to that documented for graphene or CNTs. This work provided important hints for devising optimized architecture in macroscopic assemblies, and the rich functionalities of titania promises fibers with limitless promise for a wealth of innovative applications.

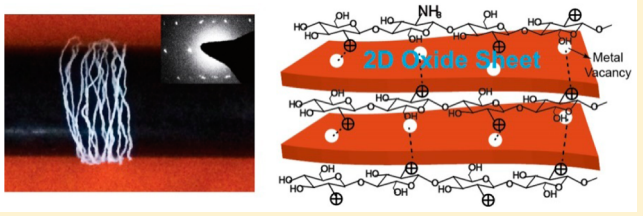

INTRODUCTION

Inorganic two-dimensional (2D) nanosheets, i.e., 2D atomic crystals having subnanometer thickness but infinite periodicity in the other two planar directions, are stimulating unprecedented scientific and technological interest as they often exhibit exotic physicochemical properties radically different from those of their bulk counterparts.[1,2] As a result, 2D nanosheets are highly interesting building blocks for creating advanced structures and novel functional materials, among which the creation of macroscopic fiber is particularly an alluring goal.[3−6] The integration of nanoscale sheet material into macroscopic structure would on one side bring enhanced behaviors owing to the cumulative effect of individual nanostructure components and on the other serve as an effective bridge from nanoscopic to macroscopic scale, offering easiness for handling in devices etc. Additionally the subject material in fiber form possesses great potential uses in future smart clothing and wearable electronic devices. For example, motivated by the exceptional physical and chemical properties of graphene, the scientists spared no effort to align graphene (oxide) into macroscopic fiber, mainly by strategies either of the industrially viable wet-spinning method, which involves injecting graphene oxide colloid solution into a coagulation bath,[5,7] or of a dimension-confined hydrothermal approach, hydrothermally treating graphene solution in a fiber-shape container, for example, glass pipeline.[6,8] While maintaining the general characteristics of mechanical flexibility for conventional fibrillar materials, the obtained fiber was unique in possessing a repeated layer stacking morphology, which endows the material with numerous possibilities for novel architecture design, for example, hybridization with branched polymers, functional particles etc.[8,9] Moreover, the attempts to make fibers of CNTs, a rolled-up structure of graphene, have been never ceased ever since the first report of CNT fiber in 2000,[10] endlessly pursuing an even better functionality combination of mechanical strength with electrical and thermal conductivity.[11] The research enthusiasm has been mainly originated from the theoretical ultrahigh elastic modulus and unsurpassed strength for pristine or defect-free graphene, honeycomb arrangement of sp^2-bonded carbon, which is

Received: August 28, 2015
Published: September 22, 2015

DOI: 10.1021/jacs.5b09138
J. Am. Chem. Soc. 2015, 137, 13200−13208

Young's modulus of 1 TPa and tensile strength of over 100 GPa.[12,13] However, despite of the intrinsic rigidity, the performance levels of the currently available macroscopic fibers is still fall short of the impressive properties of individual constituents, the main culprit for which may include the marginal constituent alignment and poor connectivity between the nanocomponents. Therefore, designing microstructure with perfectly aligned nanoscale component along with strengthened interactions is an important prerequisite to the ultimate goal of achieving fibers that well inherit the features of each individual, which, however, has been thought to be an unresolvable problem.

Meantime, the research on fibers has been limited to carbon materials, like polymers, CNTs, graphene, whereas fibers of other 2D sheets have not been attempted, which, though, may provide important hints to the further advancement of the field. Regarding graphene analogue, a wide variety of 2D materials has been achieved, such as sheets of clay, hexagonal boron nitrides (*h*-BN),[14,15] transition metal dichalcogenides (MoS_2 and WS_2),[16] metal oxides (e.g., $Ti_{0.87}O_2^{0.52-}$, $Ti_{0.91}O_2^{0.36-}$, $MnO_2^{0.4-}$, $Ca_2Nb_3O_{10}^-$),[2,17] hydroxides ($Mg_2Al(OH)_6^+$),[2,18] phosphates and phosphonates ($Zr(HPO_4)_2{\cdot}H_2O$),[19] and others.[20] Particularly, metal oxide nanosheets have received significant attention in virtue of their intriguing and exciting properties, among which sheets of titanium oxide have been the most studied for their rich functionalities in catalysis, photocatalysis, electronics, photovoltaic, and also biomedical applications.[21] Functional particles of metals oxides, such as Fe_3O_4, NiO, have been integrated onto the carbon-based fiber by postdeposition to induce additional functionalities of magnetism, electrochemical activities, etc., which, however, brought additional operational complexity and typically result in deterioration of fiber strength.[22,23] That macroscopic fiber of neat metal oxides was not available may be mainly blamed on the intrinsic low mechanic stiffness of metal oxides, only few hundredths of that for graphene.[24]

Here, using titania sheets as an illustrating example, we demonstrate, for the first time, the successful fabrication of macroscopic fiber with sheets of metal oxides. Considering the good dispersibility of metal oxide sheets in aqueous media, wet-spinning approach was adopted for the purpose. Regardless of the fact that the theoretical stiffness for molecular sheets of $Ti_{0.87}O_2^{0.52-}$ was only a small percentage of that for graphene, the unusually highly ordered stacking of sheets coupled with solid connections between the sheets endowed the fiber with tensile strength of 160 MPa and elastic modulus of 15.4 GPa, which was even comparable with graphene counterpart. The work would provide general hints to constructing optimal architecture for macroscopic fibers and more importantly offer numerous new possibilities for novel fiber functionalizations.

EXPERIMENTAL SECTION

Preparation of Titania LC Dispersions. Titania sheets were prepared by the protocol described previously.[25] Layered potassium lithium titanate with composition of $K_{0.8}[Ti_{1.73}Li_{0.27}]O_4$ were first produced by a high-temperature solid-state growth method. Chemicals of TiO_2, K_2CO_3, and Li_2CO_3, were mixed intimately in a molar ratio of 10.4:2.4:0.8, and the mixture was loaded in a Pt crucible to react at 1173 K for 20 h. The titanate microcrystals of $K_{0.8}[Ti_{1.73}Li_{0.27}]O_4$ were recovered and following converted into the protonic form through leaching in HCl by stirring in a 0.5 mol·dm^{-3} HCl solution at ambient temperature for 2 days with the acid solution replaced with a fresh one every the other day. The protonated product, $H_{1.07}Ti_{1.73}O_4$, was collected by filtration, washed with copious quantities of water and ethanol, and air-dried. For producing single-layer titania LC dispersions, a certain amount of protonic titanate crystals were immersed in tetramethylammonium hydroxide solution ($(CH_3)_4NOH$; TMAOH), the concentration of which corresponded to a molar ratio of 1:1 with respect to exchangeable protons in the titanate materials. The solid-to-solution ratio was 4 g/L.

Preparation of Titania Fiber. For spinning the nanosheet colloidal suspension into fiber, the obtained titania sheet dispersion was loaded into a glass syringe and slowly injected into coagulation bath, inorganic metal ions of different valence and organic cations with various geometry, among which chitosan in aqueous acetic acid solution (0.6−1.6% chitosan, 4% acetic acid) produced the optimal fiber. The coagulation bath was located on a rotating disk to induce a tensile force on the freshly flocculated fiber, thereby improving constituent alignment. The solution injection rate and the rotating speed should be carefully adjusted to obtain continuous fiber. After finishing spinning, the fiber was typically soaked in the bath for a certain period to ensure complete infiltration of coagulation formulations into the fiber before washing with ethanol and water to remove excessive chitosan and drying at room temperature.

Characterizations. The wide-angle X-ray diffraction (XRD) diagrams were collected on a Rigaku Ultima IV powder diffractometer with graphite monochromatized Cu Kα radiation (λ = 0.15405 nm). Lateral dimensions and thickness of exfoliated nanosheets were characterized using tapping-mode atomic force microscope (AFM; Bruker Instruments Dimension Icon) with a silicon-tip cantilever (40 N m^{-1}), for which the titania nanosheets were deposited on a mica substrate. Polarized optical microscopy for nematic LC phase of titania sheets and also the spun fiber was carried out on an Olympus IX73 apparatus. Scanning electron microscope (SEM) images were taken on a S-4700 microscope. Ultrathin sections were cut with a diamond knife on an EM UC6 ultramicrotome (Leica-Reichert) and mounted onto Formvar/carbon-coated copper grids. The sections were examined with a FEI Tecnai G2 F20 S-Twin transmission electron microscope (TEM) at an acceleration voltage of 200 kV. Thermogravimetric (TG) analyses were conducted on TG 209 F1 Libra instrument using flowing air with a ramp rate of 10 °C/min from room temperature to 800 °C. Fourier transform infrared spectroscopy was performed on a Bruker VERTEX70 FT-IR spectrophotometer over the wavenumber range of 4000−400 cm^{-1}. The light source was unpolarized. The tensile mechanical properties of the fibers with a length of 6 mm were measured on a tensile testing instrument (Instron 3365) at a strain rate of 0.1 mm·min^{-1}.

RESULTS AND DISCUSSION

Unilamellar Titania Nanosheets. Titania was chosen for a representative study because it has been one of the most studied materials during the past tens of years due to its ever-growing variety of applications in modern technology ranging from photocatalysis, solar cell, to batteries and others.[21] Titania sheets of variable compositions were available with the general composition of $Ti_{1-\delta}O_2^{4\delta-}$ ($0<\delta<1$).[21,26] In our quest for perfectly ordered sheet-stacking structure with strong sheet interactions, we need to consider sheets those satisfy two criteria: (1) the sheet bears high charge density to maximize the sheet-to-sheet interactions, and (2) dispersion of the sheet should demonstrate liquid crystalline (LC) feature, in which the molecular self-orientation would promote the formation of ordered microstructure in the resultant macroscopic material, as is the case for rod-like polymer, CNTs, and also graphene.[7,10] Among the several known titania sheets, $Ti_{0.87}O_2^{0.52-}$ has relatively large charge density of 9.38 nm^{-2} occurred by the increased percentage of Ti vacancy, in sharp contrast with the low value of 0.4 nm^{-2} for GO sheet[27] that is mostly served as precursor for preparing graphene fiber due to its good solvent dispersibility. Meantime, anisotropic fluids of $Ti_{0.87}O_2^{0.52-}$ having liquid crystalline (LC) feature was demonstrated and

DOI: 10.1021/jacs.5b09138
J. Am. Chem. Soc. 2015, 137, 13200−13208

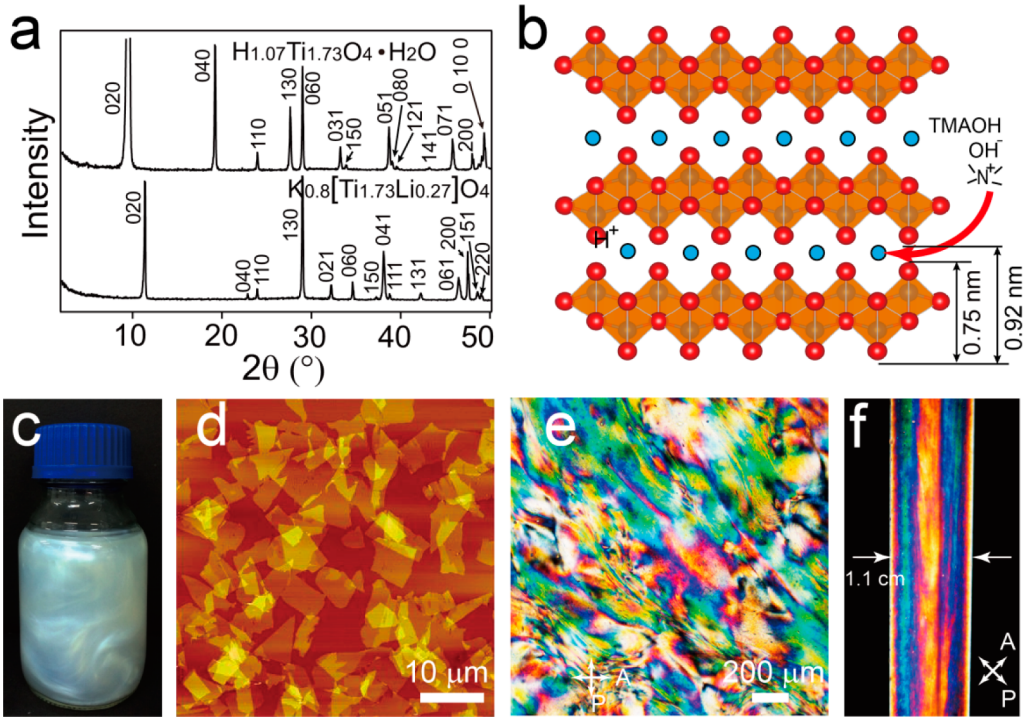

Figure 1. Characterizations of the protonated titanate precursor and LC nature of the exfoliated titania sheets. (a) XRD patterns for the starting $K_{0.8}Ti_{1.73}Li_{0.27}O_4$ and protonated $H_{1.07}Ti_{1.73}O_4{\cdot}H_2O$ crystals. (b) A simple illustration for the intercalation of TMAOH along with H_2O molecules into the gallery between stacked $Ti_{0.87}O_2^{0.52-}$ sheets, which would finally result in exfoliation into single-layer nanosheets. The crystallographic thickness of an individual layer is 0.75 nm. (c) Digital photograph of the exfoliated colloidal solution showing shiny textures typical of a nematic LC mesophase. (d) Tapping-mode AFM image of the delaminated sheets. The surface was smooth and the thickness was estimated to be 1.1 nm, indicating the unilamellar feature of the sheets. Optical microscopic images for the nanosheet LC colloid taken between crossed polarizers: (e) of one drop on a glass plate giving typical birefringent Schlieren textures, and (f) in a tube with diameter of 1.1 cm after standing for several minutes showing that at an external shear force the sheets could orient along the tube wall direction on a macroscopic centimeter scale.

the formation mechanism was systematically studied by us lately.[28,29] Therefore, for this study, we employed LC colloid of $Ti_{0.87}O_2^{0.52-}$ sheets disintegrated from microcrystalline precursor of $K_{0.8}Ti_{1.73}Li_{0.27}O_4$, the crystal structure of which consisted of repeated stacking of $[Ti_{1.73}Li_{0.27}O_4]^{0.8-}$ layers with K^+ residing in the gallery to neutralize the unbalanced charges. The synthesis procedure involved a typical three-step flow, first high-temperature solid-state growth of parent microcrystals $K_{0.8}Ti_{1.73}Li_{0.27}O_4$, then extraction of both alkali metal ions (potassium and lithium) by acid-leaching, and finally reaction with base solution under mechanical shaking conditions (synthesis details in Experimental Section). As usually observed for materials possessing a layered structure, the so-obtained product for $K_{0.8}Ti_{1.73}Li_{0.27}O_4$ was grown into plate-like crystallites, with lateral dimensions and thickness averaged to be 6−8 μm and hundreds of nanometers, respectively (Supporting Information). After transforming to the protonated form, $H_{1.07}Ti_{1.73}O_4{\cdot}H_2O$, in HCl, the plate crystals became to some extent loosened accompanied by an obvious left shift of basal reflection, which was due to the replacement of K^+ in the gallery and Li^+ in the layer with protons. All the peaks in the respective X-ray diffraction (XRD) patterns depicted in Figure 1a could be well indexed in an orthorhombic cell, with lattice dimensions refined to be a = 0.38255(6), b = 1.55291 (33), c = 0.29179(7) nm for potassium precursor and a = 0.37873(7), b = 1.84518 (6), c = 0.29942(9) nm for protonated crystals. The subsequent expansion of layers, i.e., swelling, and exfoliation of titanate materials have been thoroughly studied, which proved that dimensions of exfoliated sheets and the resultant solution phase, isotropic or anisotropic, could be delicately controlled by adjusting conditions such as electrolyte identity, electrolyte concentration, and shear forces.[28,29] The formation of LC phase for lamella minerals was first discovered for $H_2Sb_3P_2O_{14}$, which was generated by the long-range nanometer-scale ordering of the planar sheets in water.[30] To produce the desired titania LC phase, we employed tetramethylammonium hydroxide (TMAOH) as the electrolyte and its concentration was in a molar ratio of 1:1 relative to the exchangeable protons in the used titanate materials. As illustrated in Figure 1b, reaction of the protonated titanate with TMAOH aqueous solution would bring intercalation of TMA^+ along with H_2O molecules, which significantly weakened the binding forces between the layers and thereby resulted in exfoliation of the layered titanate into molecular sheets. Reaction of the protonated crystals in TMAOH solutions under mechanical shaking led to the final complete exfoliation, and the suspension of 4 g/L manifested an appearance of shiny textures (Figure 1c and Supporting Information), suggesting the presence of quasi-long-range molecular order and formation of a nematic LC mesophase. Atomic force microscope (AFM) analysis confirmed that the substance in the colloidal solution was indeed monolayer sheets with a measured thickness of ~1.1 nm (Figure 1d), in accordance with a sum of the crystallographic value for one single titania layer, 0.75 nm, and an unavoidable surface adsorption of electrolyte TMA^+. A comprehensive survey on 247 sheets taken at 5 different spots showed that the lateral dimensions for the majority of sheets were in the domain of several micrometers and a statistical

DOI: 10.1021/jacs.5b09138
J. Am. Chem. Soc. 2015, 137, 13200−13208

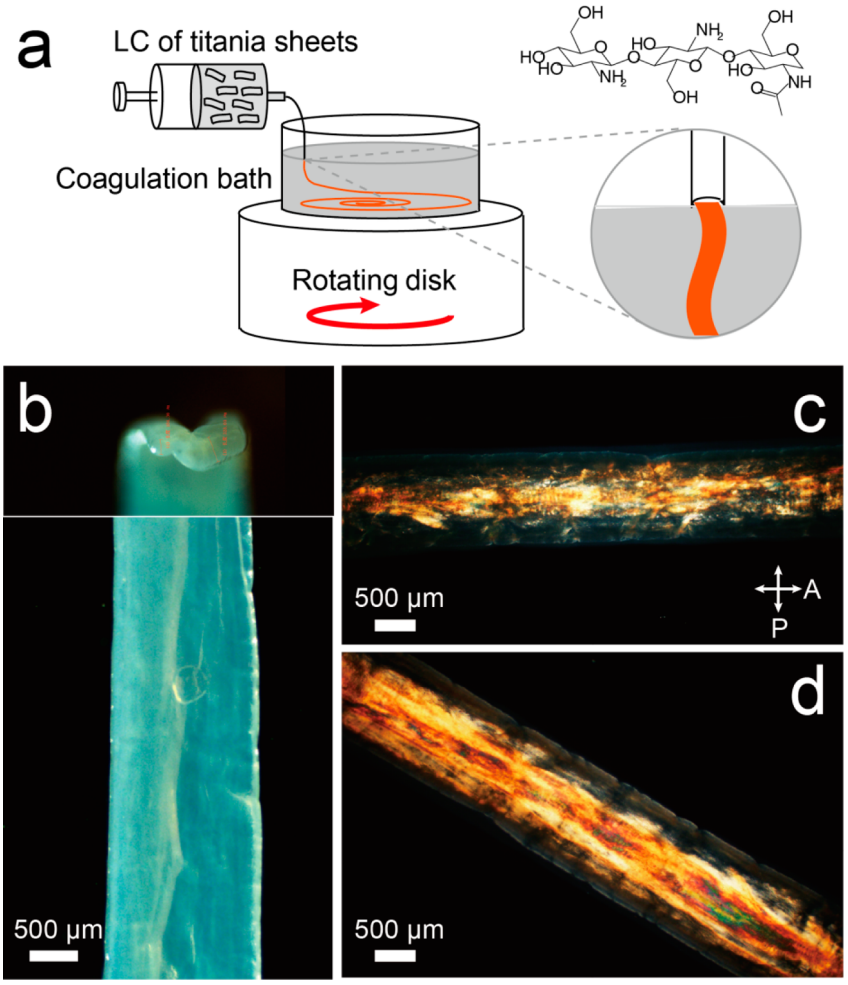

Figure 2. Characterizations of the as-obtained titania fiber. (a) A schematic apparatus for the wet-spinning of titania fibers. The LC dope was kept in a syringe and injected into a flocculation solution, which was rotating at a certain speed. Inset: molecular structure of optimal coagulant, chitosan, having amino group, -NH_2, on each saccharide ring, which could be protonated and bear positive charges in acids. (b) Dark field illumination for the fiber of ribbon morphology with width of ∼1300 μm and thickness of ∼200 μm. Microscopic image of the ribbon fiber between crossed polarizers at (c) 0° and (d) 45°angle with the polarizer. The directions of polarizer and analyzer are indicated by the double arrows, *P* and *A*, respectively.

analysis gave an average value of 6 μm (details in Supporting Information). Figure 1e shows a representative optical microscope image for one drop of the titania sheet colloid observed between crossed polarizers, manifesting vivid birefringent Schlieren textures, which unambiguously proved the successful formation of nematic LC phase and preordering of the titania sheets. Furthermore, the colloid in a tube (diameter 1.1 cm) after standing for several minutes showed homogeneous colors along the tube wall, as observed in Figure 1f, indicating that at an external shear force the titania sheets could macroscopically orient along the wall on the centimeter scale, which offered strong basis for spinning well-aligned macroscopic fibers.

Solution-Spinning of Ribbon Fiber with Well-Aligned Stacking Structure. For attaining the purpose of producing macroscopic fiber from LC of titania sheets, wet-spinning approach was chosen as this technique has many advantages such as being simple, economic, scalable, and has been industrially utilized to fabricate many a kind of fibers including rayon, Kevlar, polyaniline, CNTs, graphene, and numerous others. Using an analogous methodology previously done for producing these fibers, an aqueous titania suspension with a concentration of 4 g/L was extruded through a needle with diameter of 900 μm by a syringe pump into an aqueous coagulation solution placed on a constantly rotating stage, the configuration for which is illustrated in Figure 2a. The flowing of the coagulation bath has been believed to be critical in helping improve the constituent alignment in the result fiber. Considering $Ti_{0.87}O_2^{0.52-}$ titania sheet bears negative charges of high density, 9.38 nm^{-2} in sharp contrast with 0.4 nm^{-2} of GO, various coagulant formulations, including metal ions of different valence and macromolecules of different geometry having positive charges, such as NaCl, $CaCl_2$, $LaCl_3{\cdot}6H_2O$, cetyltrimethylammonium bromide, chitosan, etc., were attempted (Supporting Information). For all cases, once on contact of the coagulant in the bath, the spinning sheet solution destabilized and transformed into a dense gel fiber in white due to an immediate ionic complexation between the negatively charged spinning dope and positively charged coagulant, among which the use of chitosan in aqueous acetic acid medium resulted in optimal fiber. The molecular structure of chitosan, a partially deacetylated product of chitin, is given in inset of Figure 2a, a straight-chain polysaccharide consisting of D-glucosamine and *N*-acetylglucosamine units linked through 1−4 glycosidic bonds, which in acidic media is a polyelectrolyte with the protonation of amino group, -NH_2, on each D-unit. Although

DOI: 10.1021/jacs.5b09138
J. Am. Chem. Soc. 2015, 137, 13200−13208

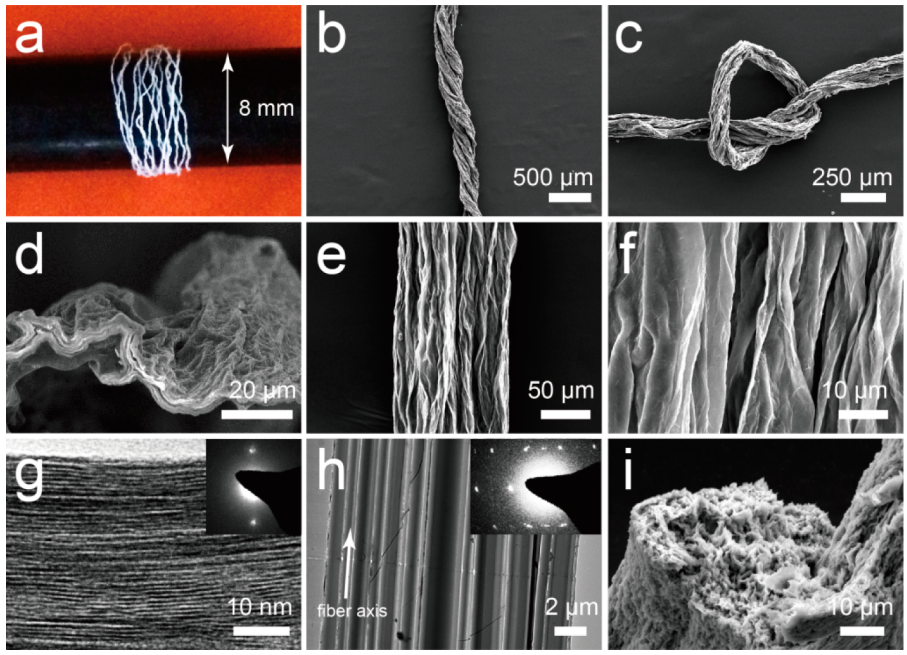

Figure 3. Microscopic structural characterization of the titania fiber. (a) Photograph of dried fiber of 38 cm in length wound on a spool with diameter of 8 mm. SEM images of (b) bundle twisting and (c) knotting titania fibers. No damage or cracks were detected, revealing the high flexibility and resistance to torsion of the titania fiber. (d) Cross-section view and (e, f) surface morphology for the fiber. The sheets were fused without obvious observation of discrete sheets, although the surface was wrinkled on some degree. (g) Cross-sectional HRTEM lattice image of a chitosan-fiber slice and the corresponding SAED pattern (inset), showing the unusual nearly perfect cofacial stacking of the 2D titania sheets. (h) TEM image for the fiber sliced along the ribbon plane. Inset: SAED pattern for the sheet stacks. The observation of only one set of diffractions signified probable existence of sheet registry. (i) SEM morphology view for the fiber spun with La^{3+} manifesting intertwined sheets and fluffy surface.

there have been a few examples of spinning GO sheets with chitosan into composite films or fibers in which chitosan served as efficient fillers in improving fiber strength,[31,32] the complexation with $Ti_{0.87}O_2^{0.52-}$ sheets in this study was far beyond previous reports with possible site-specific connection and formation of a hybrid with unusually well-aligned sheet-stacking (vide post). Because of the ready spinnability of the sheet suspension, continuous and long fiber could be obtained as long as the feed stock allowed. After thorough repeated washing with water and ethanol and subsequent drying in ambient conditions, flexible and strong enough fiber was obtained so that it could be wound around a spool (Figure 3a). The drawn fibers were cut into smaller segments for all later characterizations. Despite of the known low stiffness of molecular titania sheets, which was only a minor percentage of that for graphene sheets, the so-obtained titania fiber was as flexible and rigid as the reported CNT/graphene fibers. The fiber could be twisted or tightly knotted without the occurrence of any breakage (Figure 3b,c), demonstrating excellent flexibility and enough resistance to torsion of the fibers compared with the classical carbon fibers. Furthermore, owing to the superior flexibility, the titana fiber could be used to weave pure titana fabrics or embroidery patterns, for example, Chinese character of our city, *SU*, in usual textiles (Supporting Information).

Optical microscope was used to examine the fiber morphology and microscopic alignment of sheets in the fiber. Differing from the circular cross-section for most documented CNT/graphene fibers spun in a similar setup, the as-obtained fiber in wet state was in a flat ribbon-like morphology, with a typical width of ~1300 μm and thickness of 200 μm (Figure 2b). If the titania sheets were ideally in situ flocculated with chitosan along with water at the exit of needle, the width and thickness would be dictated by the confinement of the syringe outlet, which would have given much thicker fiber. Therefore, the interdistance between the sheets was much condensed in the solution-spinning or polyionic complexation process. The dense stacking of the constituent nanosheets, along with large shear fluid flow velocity compared to the injection rate of nanosheet suspension, may be mainly responsible for the formation of the ribbon shape. Under crossed polarizers shown in Figure 2c,d, the fiber displayed interference colors due to the birefringence of the sample. The color was nearly homogeneous and the transmitted light intensity was dependent on the relative orientation of the ribbon with respect to the optical axis of the polarizers, suggesting that the alignment of the sheets in the flow was preserved and predominantly oriented along the axis of fiber. The titania ribbon fiber was dried by suspending in ambient conditions with the two extremities hung on solid objects, during which macroscopic ribbon in all the three dimensions shrank significantly due to the water loss while maintaining the sheet alignment feature. The fiber length could be subtly adjusted by changing the distances between the two ends, and one-end free ribbon was found to shrink by approximately 6% (Supporting Information); width and thickness contracted to 250 and 20 μm, respectively, as evidenced by scanning electron microscope (SEM) observations.

The microscopic features of the dry-state titania fiber were further examined with electron microscopic characterizations. Figure 3d–f are typical SEM morphology images for cross-section and surface at various magnifications. The ribbon shape was maintained after drying. Notably, the surface was relatively smooth across the whole fiber without any obvious discerning of sheet edges and cracks, suggesting completely compact stacking and possible coalescence, as reported in synthesizing

DOI: 10.1021/jacs.5b09138
J. Am. Chem. Soc. 2015, 137, 13200–13208

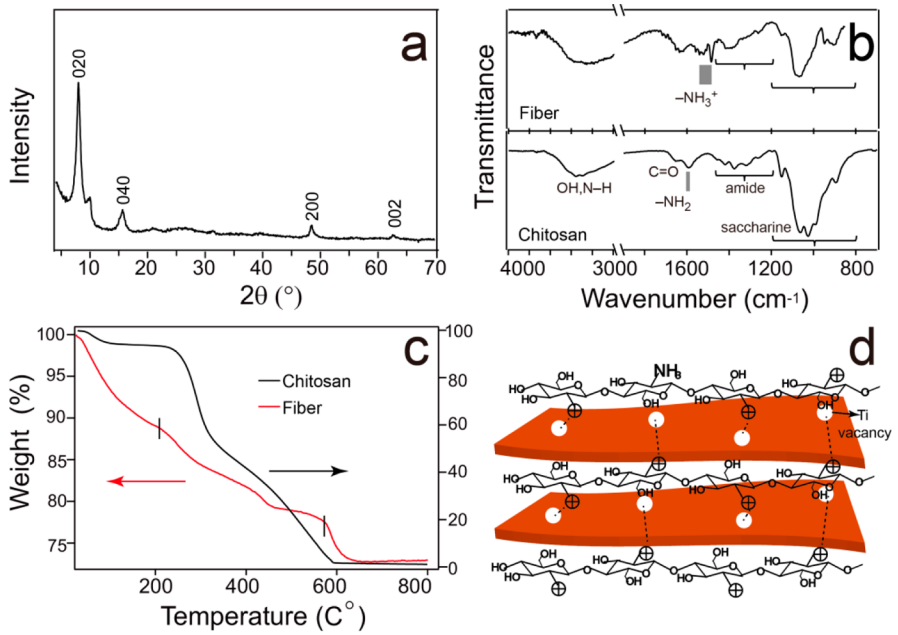

Figure 4. Spectral analysis of the fiber structure. (a) An example of XRD pattern of the fiber showing sharp basal reflections, in-plane ones, and a few others, suggesting the long-range stacking order in the obtained fiber. (b) FT-IR spectrum for the titania fiber compared with that for pure chitosan. The band corresponding to $-NH_2$ in pure chitosan shifted to low-energy region, evidencing for the protonation and electrostatic interaction with titania sheets. (c) TG curve for the fiber, from which the formula was determined to be $(Ti_{1.73}O_4)^{1.07-}(C_6H_{12}NO_4^+)_{0.24}(H^+)_{0.83}\cdot 2H_2O$. The chitosan content in the fiber was in line with population of Ti vacancy in titania sheet unit, $Ti_{1.73}\square_{0.27}O_4$ ($\square$ represents vacancy), i.e., 0.27. (d) An illustration of the possible fiber structure, protonated chitosan electrostatically interacted with the specific Ti vacancy site in titania sheets, giving a fiber with well-aligned stacking structure.

CNT fiber, which could efficiently prevent fiber breakage thereby improving toughness of the fiber. The crumbles or wrinkles on the surface should result from some degree of folding due to the minimization of surface energy driven by water loss in the drying process. Cryo-cut was conducted following, for a closer inspection of the sheet-to-sheet stacking. Figure 3g is a high-resolution transmission electron microscopy (HRTEM) lattice image for cross-section, showing clear parallel fringes, which revealed that the sheets were unidimensionally orientated along the fiber axis direction and cofacially glued to each other with no obvious observation of voids. The interplane spacing was measured to be 1.1 nm, accorded with the basal spacing in XRD study (vide post). The TEM image for fiber sliced along the ribbon plane is given in Figure 3h, further evidencing the aligned stacking of sheets. Importantly, the corresponding selected area electron diffraction (SAED) pattern of the sheet stacks (inset) manifested only one set of diffraction spots, signifying that sheet registry might exist between neighboring sheets and, in other words, the sheets probably stacked in an unusual quasi-crystalline manner. In sharp contrast, the surface of fibers spun with inorganic ions, Na^+, Ca^{2+}, La^{3+}, etc., was fluffy and the sheets were severely intertwined (Figure 3i), suggesting that aligning and sheet-to-sheet registry was absent in these fibers, which resulted in ready breakage. For the chitosan-complexed fiber, owing to the large-scale sheet alignment, cofacial dense stacking, and strong sheet-to-sheet interactions, the titania fiber was robust and flexible enough so that it could be easily wound around a spool, twisted into a bundle yarn, tied into a knot, and even loaded a burden of 50 g without the appearance of any cracks or breakage (Figure 3a–c and Supporting Information).

The fiber was subsequently subjected to structural analysis in detail, which revealed that the fiber consisted of alternative stacking of titania sheets and chitosan, in which the sheets and chitosan was interconnected in a possible site-specific manner. A typical wide-angle XRD pattern is given in Figure 4a, displaying basal reflections characteristic of layered stacking structures, in-plane reflections of 200 and 002 at approximately 48.5° and 62.7°, and a few other lines. The basal reflections were very sharp, indicating a long-range ordering of the assembled sheets along the stacking direction. The repeated distance for the stacking was estimated to be 1.13 nm. As the interaction between titania sheets and chitosan was mostly electrostatic interaction, it was reasonable to assume the wagged saccharide ring was positioned parallel to the sheets with the protonated $-NH_3^+$ group pointing perpendicular to the sheets. The dimension for chitosan flat-lying in the gallery was ~0.4 nm, and consequently the periodic spacing for the lamellar structure, the added value of chitosan with crystallographic thickness of titania sheets, could be estimated as 1.15 nm, in good consistence with XRD studies. The presence of interaction between titania sheets and chitosan was confirmed by Fourier transform infrared spectroscopy (FT-IR) study. Figure 4b shows the IR spectrum of titania sheets-chitosan fiber compared with that for pure chitosan powder in the 4000–750 cm^{-1} range, in which no appreciable difference was observed in characteristic signals for saccharine, amide group CONHR, and OH of chitosan (Supporting Information). A noteworthy feature was that the absorption for $-NH_2$ at 1591 cm^{-1} became no longer noticeable after complexation, accompanying occurrence of peaks in lower wavenumber region, which should be associated with the protonation of amino group and the electrostatic interaction with titania sheets. In addition, thermogravimetric (TG) analysis was performed to achieve the relative weight percentage of titania sheets and chitosan with the spectrum depicted in Figure 3c along with that for

DOI: 10.1021/jacs.5b09138
J. Am. Chem. Soc. 2015, 137, 13200–13208

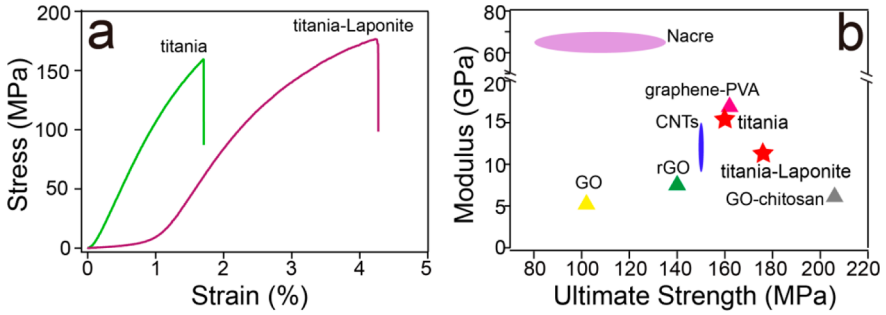

Figure 5. Mechanical measurements of the titania fiber. (a) Stress−strain curves for titania and titania-Laponite fibers. (b) A mechanical performance comparison of the novel titania fiber with some typical documented materials. Although the inherent strength of molecular titania sheets was only a small fraction of that for CNT/graphene, the mechanical properties of titania fiber were competent, thanks to the optimized crystalline compact stacking architecture.

pure chitosan for comparison purposes. The weight loss was at 3 different steps, sequentially ascribing to removal of physisorbed and crystalline H_2O, decomposition of intercalated chitosan, and phase transformation of $Ti_{0.87}O_2^{0.52-}$ to TiO_2. Unexpectedly, the protonated chitosan could not completely compensate the negative charges on titania sheets. Considering that coagulant electrolyte was chitosan in aqueous acid, H^+ was used to neutralize the unbalanced charges and the formula for the fiber was consequently written as $(Ti_{1.73}O_4)^{1.07-}(C_6H_{12}NO_4^+)_{0.24}(H^+)_{0.83}\cdot 2H_2O$. The chitosan amount relative to titania sheet unit, $[Ti_{1.73}O_4]$, was so little as 0.24, that is, only one deacetylated glucosamine unit in every 4 titania unit cells with a planar area of 0.456 nm^2 (= 0.38 × 0.30 × 4 nm^2). This could be possibly explained by steric effect with the ring-projected area of chitosan comparative to that of 4 units of molecular titania sheets (Supporting Information). To examine if geometry limitation was the determining factor, composition of fiber spun with Na^+ possessing ionic radii as low as 0.1 nm was also checked, which gave a similar formula, $(Ti_{1.73}O_4)^{1.07-}Na^+_{0.27}(H^+)_{0.8}\cdot 2H_2O$, thus excluding the sole or dominant control of geometrical limitations.

Meantime, the chitosan or Na^+ content in the fiber reminded us the population of Ti vacancy relative to titania sheet unit, $[Ti_{1.73}\square_{0.27}O_4]^{1.07-}$ (□ represents vacancy), was almost of the same value, that is, 0.27, which, we believe, was not an accidental coincidence and instead a hint indicating that the protonated chitosan was most likely electrostatically bonded to the specific Ti vacancy site where negative charges should have been concentrated. The electrostatic interaction of the Ti vacancy with the protonated $-NH_3^+$ on every saccharide ring was localized at specific sites and accordingly would fix the sheets, preventing possible sliding and rotating of the sheets, which finally resulted in a highly ordered structure (Figure 4d), as experimentally evidenced by TEM microstructural characterizations (vide ante). Even the chitosan concentration was doubled or tripled, neither the amount of intercalated chitosan nor the basal spacings exhibited obvious changes, with TG and XRD results provided in Supporting Information, which further supported that the fiber was composed of a crystalline compound with a fixed formula, rather than a composite of two separate components having variable compositions. The high degree order of the sheets and the strong binding interactions would be beneficial to efficiently translating nanoscale attributes to a macroscopic object and accordingly fully utilizing the potential of nanoscale components.

Mechanical Performances of the Obtained Fiber. Regardless of the intrinsically low stiffness of titania sheets, elastic constants of which was calculated to be 30−150 GPa,[24] far inferior to nearly 1 TPa of graphene,[12] the obtained macroscopic fiber displayed competent mechanical properties. The three important gauges for mechanical properties, i.e., tensile strength, modulus, and elongation at fracture were determined from mechanical tensile measurements on macroscopic individual filaments of ∼6 mm long with stress−strain curve given in Figure 5a. Stress was calculated from the ratio of applied force to the fiber cross-sectional area determined by SEM or optical microscopy. Tensile measurements showed that the fiber displayed linear elastic behavior with no occurrence of any yield, which may be due to the strong glue forces between the neighboring sheets. The maximum tensile strength was up to 160 MPa at elongation of 1.7%. The Young's modulus could be estimated from the slope of stress−strain curve, which was 15.4 GPa. Clay has been known to have a natural house-of-cards type structure in aqueous solutions, the inclusion of which into composite film would generally increase the mechanical performances. By introducing a minor amount of Laponite into the starting titania LC dope, a titania-Laponite composite fiber was produced with a similar procedure. The mechanical strength and Young's modulus manifested little changes, optimal strength increased 10% to 176 MPa and Young's modulus to 11.3 GPa, which could likely be explained by the fact that the original titania fiber was aligned and compact enough. A noteworthy feature was that the titania-Laponite fiber under tensile loading exhibited a typical plastic deformation at room temperature and significant improvement of fracture elongation, nearly three times longer to 4.25%, which was presumably a result of displacements of Laponite sheets. The strength and modulus values were close and even superior to previously reported materials, nacre (80−135 MPa, 60−70 GPa),[33] CNTs fiber (150 MPa, 9−15 GPa),[10] GO fiber (102 MPa, 5.4 GPa),[7] rGO fiber (140 MPa, 7.7 GPa),[7] graphene-PVA composite fiber (162 MPa, 17.1 GPa),[34] and also GO-chitosan fiber (206 MPa, 6.3 GPa).[31,32] Although the inherent strength of titania sheet was much weaker than graphene, mechanical performance for the macroscopic fiber assembly was comparable, which should be endowed to the unique optimal architecture, efficient sheet-to-sheet fusion, unidimensional sheet alignment, and crystalline sheet stacking.

Fire Retardancy of the Fiber. Conventional fabrics are easily ignitable and potentially dangerous in fire, and therefore the demand for flame retardant fiber has been strong and there have been many researches and developments to improve the flame retardant polyester, which usually requires the complicated addition of flame retardants. Burning tests showed

DOI: 10.1021/jacs.5b09138
J. Am. Chem. Soc. 2015, 137, 13200−13208

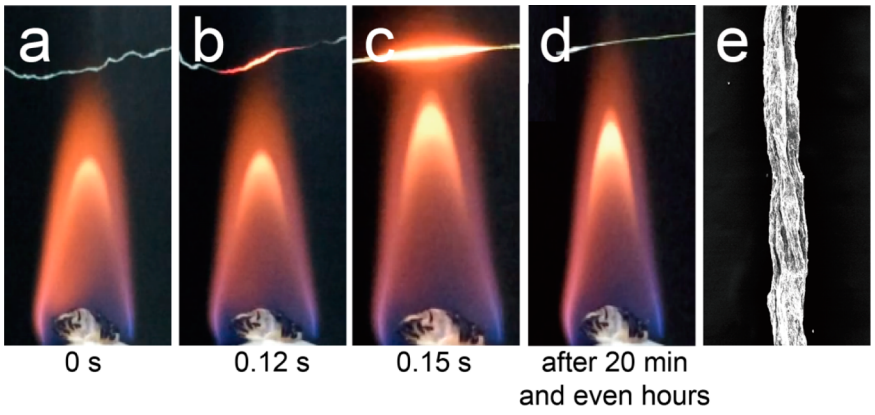

Figure 6. Flame resistance of the titania fiber. (a–d) Time-series snapshots of the titania fiber in a burning test. The fiber turned into black shortly after burning for chitosan carbonization and switched back into white also in a split second due to complete combustion of chitosan. After 20 min and even repeated hours of intense burning, the fiber integrity was well retained. (e) An SEM image of the fiber after burning experiment.

that our fiber displayed highly efficient fire retardancy. The fiber integrity could be well maintained after an extended burning of 20 min and even repeated hours of burning (video provided in Supporting Information). As the time-series snapshots presented in Figure 6a–d, the white fiber quickly turned into black when initially exposed to the flame of alcohol lamp, which was probably due to the carbonization of the intercalated chitosan. The continued burning consumed out chitosan and the fiber color reversed back to white again, after which the fiber appearance would not further show any changes even under a repeated burning of several hours (Figure 6e). Comparatively, conventional polymer fibers and graphene fibers typically burned out in seconds, and a recent report of graphene-montmorillonite composite showed that the shape did not collapse until a prolonged 15 min of burning.[35] The phase and microstructure after burning was studied by XRD and SEM characterizations (Supporting Information), which showed that the sheet stacking structure was transformed into condense aggregations of rutile TiO_2 microcrystals, which should be a result of the compact stacking structure in the original crystalline fiber. Because of the unique electronic and optical properties of titania, fiber of titania would possess many additional attributes, which have promising applications in clean energy technologies, self-cleaning, electrochemical systems, and a number of others.

CONCLUSION

We have obtained the first macroscopic ribbon fiber of semiconducting metal oxides, taking titania as an illustrating example, via a scalable wet-spinning strategy. An analogy of graphene, 2D molecular sheet of $Ti_{0.87}O_2^{0.52-}$, was employed for this purpose due to its multifuntionalities and consequently the wide potential uses of corresponding macroscopic assemblies. Significantly differing from the previously reported CNT or graphene fibers, in which only rough orientation order existed among the individual components, the titania fiber complexed with chitosan possessed unusually high order of sheet stacking with enhanced sheet-to-sheet interactions, which should be ascribed to the unique defect structure and high charge density of $Ti_{0.87}O_2^{0.52-}$. Although it is generally known that molecular sheets of metal oxides are much weaker compared with CNTs/graphene, the fiber manifested comparable and even superior mechanical performances compared with graphene analogue due to the optimal structural architecture. Considering the wide applications of titania, the titania fibers and textiles would find a variety of promising applications, particularly in green and wearable devices for self-cleaning, energy storage, etc. Revolutionarily realizing fiber of noncarbon, functionality-rich metal oxide materials through highly ordered assembly, this study provided important hints for optimized construction of macroscopic architecture and meantime opened a new window onto making macroscopic fibers of general 2D crystals with numerous functionalities.

ASSOCIATED CONTENT

Supporting Information

The Supporting Information is available free of charge on the ACS Publications website at DOI: 10.1021/jacs.5b09138.

More SEM, AFM images, fiber dimension change in the drying process, size comparison of chitosan with titania sheet, XRD and TG data for fiber coagulated with concentrated chitosan, phase identification and morphology characterization for fiber after burning. (PDF)

Video of resistant fiber combustion for 20 min. (AVI)

AUTHOR INFORMATION

Corresponding Authors

*zgzhao2011@sinano.ac.cn

*gengfx@suda.edu.cn

Notes

The authors declare no competing financial interest.

ACKNOWLEDGMENTS

The authors acknowledge financial support from the National Natural Science Foundation of China (51402204), Thousand Young Talents Program, Jiangsu Specially-Appointed Professor Program, and a project funded by the Priority Academic Program Development (PAPD) of Jiangsu Higher Education Institutions. Dr. Z. G. Zhao is thankful for support by the National Natural Science Foundation of China (51372266 and 51572286).

REFERENCES

(1) Novoselov, K. S.; Jiang, D.; Schedin, F.; Booth, T. J.; Khotkevich, V. V.; Morozov, S. V.; Geim, A. K. *Proc. Natl. Acad. Sci. U. S. A.* **2005**, *102*, 10451.

(2) Ma, R.; Sasaki, T. *Acc. Chem. Res.* **2014**, *48*, 136.

DOI: 10.1021/jacs.5b09138
J. Am. Chem. Soc. 2015, 137, 13200–13208

(3) Wicklein, B.; Kocjan, A.; Salazar-Alvarez, G.; Carosio, F.; Camino, G.; Antonietti, M.; Bergström, L. *Nat. Nanotechnol.* **2015**, *10*, 277.
(4) Liu, M.; Ishida, Y.; Ebina, Y.; Sasaki, T.; Hikima, T.; Takata, M.; Aida, T. *Nature* **2015**, *517*, 68.
(5) Xu, Z.; Gao, C. *Acc. Chem. Res.* **2014**, *47*, 1267.
(6) Cheng, H.; Hu, C.; Zhao, Y.; Qu, L. *NPG Asia Mater.* **2014**, *6*, e113.
(7) Xu, Z.; Gao, C. *Nat. Commun.* **2011**, *2*, 571.
(8) Hu, C.; Zhao, Y.; Cheng, H.; Wang, Y.; Dong, Z.; Jiang, C.; Zhai, X.; Jiang, L.; Qu, L. *Nano Lett.* **2012**, *12*, 5879.
(9) Hu, X.; Xu, Z.; Gao, C. *Sci. Rep.* **2012**, *2*, 767.
(10) Vigolo, B.; Pénicaud, A.; Coulon, C.; Sauder, C.; Pailler, R.; Journet, C.; Bernier, P.; Poulin, P. *Science* **2000**, *290*, 1331.
(11) Behabtu, N.; Young, C. C.; Tsentalovich, D. E.; Kleinerman, O.; Wang, X.; Ma, A. W. K.; Bengio, E. A.; ter Waarbeek, R. F.; de Jong, J. J.; Hoogerwerf, R. E.; Fairchild, S. B.; Ferguson, J. B.; Maruyama, B.; Kono, J.; Talmon, Y.; Cohen, Y.; Otto, M. J.; Pasquali, M. *Science* **2013**, *339*, 182.
(12) Geim, A. K.; Novoselov, K. S. *Nat. Mater.* **2007**, *6*, 183.
(13) Zandiatashbar, A.; Lee, G.-H.; An, S. J.; Lee, S.; Mathew, N.; Terrones, M.; Hayashi, T.; Picu, C. R.; Hone, J.; Koratkar, N. *Nat. Commun.* **2014**, *5*, 3186.
(14) Zhi, C.; Bando, Y.; Tang, C.; Kuwahara, H.; Golberg, D. *Adv. Mater.* **2009**, *21*, 2889.
(15) Kovtyukhova, N. I.; Wang, Y.; Berkdemir, A.; Cruz-Silva, R.; Terrones, M.; Crespi, V. H.; Mallouk, T. E. *Nat. Chem.* **2014**, *6*, 957.
(16) O'Neill, A.; Khan, U.; Coleman, J. N. *Chem. Mater.* **2012**, *24*, 2414.
(17) Schaak, R. E.; Mallouk, T. E. *Chem. Mater.* **2000**, *12*, 3427.
(18) Li, L.; Ma, R.; Ebina, Y.; Iyi, N.; Sasaki, T. *Chem. Mater.* **2005**, *17*, 4386.
(19) Mallouk, T. E.; Gavin, J. A. *Acc. Chem. Res.* **1998**, *31*, 209.
(20) Nicolosi, V.; Chhowalla, M.; Kanatzidis, M. G.; Strano, M. S.; Coleman, J. N. *Science* **2013**, *340*, 6139.
(21) Wang, L.; Sasaki, T. *Chem. Rev.* **2014**, *114*, 9455.
(22) Cheng, H.; Dong, Z.; Hu, C.; Zhao, Y.; Hu, Y.; Qu, L.; Chen, N.; Dai, L. *Nanoscale* **2013**, *5*, 3428.
(23) Su, F.; Lv, X.; Miao, M. *Small* **2015**, *11*, 854.
(24) Sato, H.; Ono, K.; Sasaki, T.; Yamagishi, A. *J. Phys. Chem. B* **2003**, *107*, 9824.
(25) Tanaka, T.; Ebina, Y.; Takada, K.; Kurashima, K.; Sasaki, T. *Chem. Mater.* **2003**, *15*, 3564.
(26) Ma, R.; Sasaki, T. *Adv. Mater.* **2010**, *22*, 5082.
(27) Kovtyukhova, N. I.; Ollivier, P. J.; Martin, B. R.; Mallouk, T. E.; Chizhik, S. A.; Buzaneva, E. V.; Gorchinskiy, A. D. *Chem. Mater.* **1999**, *11*, 771.
(28) Geng, F.; Ma, R.; Ebina, Y.; Yamauchi, Y.; Miyamoto, N.; Sasaki, T. *J. Am. Chem. Soc.* **2014**, *136*, 5491.
(29) Maluangnont, T.; Matsuba, K.; Geng, F.; Ma, R.; Yamauchi, Y.; Sasaki, T. *Chem. Mater.* **2013**, *25*, 3137.
(30) van der Kooij, F. M.; Kassapidou, K.; Lekkerkerker, H. N. W. *Nature* **2000**, *406*, 868.
(31) Sun, J.; Li, Y.; Peng, Q.; Hou, S.; Zou, D.; Shang, Y.; Li, Y.; Li, P.; Du, Q.; Wang, Z.; Xia, Y.; Xia, L.; Li, X.; Cao, A. *ACS Nano* **2013**, *7*, 10225.
(32) Wang, X.; Bai, H.; Yao, Z.; Liu, A.; Shi, G. *J. Mater. Chem.* **2010**, *20*, 9032.
(33) Wang, J.; Cheng, Q.; Tang, Z. *Chem. Soc. Rev.* **2012**, *41*, 1111.
(34) Kou, L.; Gao, C. *Nanoscale* **2013**, *5*, 4370.
(35) Fang, B.; Peng, L.; Xu, Z.; Gao, C. *ACS Nano* **2015**, *9*, 5214.

DOI: 10.1021/jacs.5b09138
J. Am. Chem. Soc. 2015, 137, 13200−13208